

Introduction to XRD analysis of modern functional thin films using a 2-dimensional detector

—(2) Analysis of epitaxial films

Katsuhiko Inaba*

1. Introduction

Epitaxial thin films are widely studied in the interest of fundamental scientific research into the physical properties of materials, but also due to the emerging demands of high efficiency in a wide range of industrial applications.

Among the most famous epitaxial thin films are GaN films for LED applications, the development of which led to the awarding of the Nobel Prize in Physics in 2014. The GaN heteroepitaxial films for these LEDs were grown on sapphire substrates after overcoming the large lattice mismatch between them. Though a symmetric similarity for c -axis growth of GaN (hexagonal) on the c -plane of sapphire (trigonal) exists, these two materials are totally different in the crystallographical sense⁽¹⁾. Complex domain structures and large mosaic spread (tilt/twist) of GaN epitaxial films were caused mainly by the large lattice mismatches.

In the pursuit of new characteristics comparable to GaN-LEDs, recent studies have concentrated on growing functional thin films epitaxially crystallographically different substrates. In this process, XRD analysis will be very helpful to characterize their orientation relationships, crystalline quality, etc.

The usefulness of 2D detectors for characterizing polycrystalline thin films was shown in Part 1 of this short series of articles⁽²⁾. This situation is also applicable to epitaxial thin films when 2D detectors are appropriately employed.

This article shows examples of characterizing functional epitaxial films by using multidimensional detectors, especially in 2D mode.

2. Characterization of epitaxial thin films

2.1. Measurement geometries of Reciprocal Space Maps and the dimension of multidimensional detectors

Reciprocal Space Map (RSM) measurements are often employed for the characterization of epitaxial thin films. In this section, XRD geometries for Reciprocal Space Maps (RSMs) using multidimensional detectors will be briefly explained.

A schematic drawing of XRD geometries of RSMs is shown in Fig. 1. Detailed explanations can be found in

Ref. 3 and 4.

The 2D mode of detectors is employed for wide-range RSM measurements (the area of measurement is shown in red) by tilting specimens with the χ -axis while scanning with a θ - 2θ motion (skew geometry). This measurement is performed with a point-focus incident beam.

Two types of coplanar geometries where specimens are tilted using the ω -axis should be discussed, depending on whether the ω angles are smaller or larger than half of 2θ .

When the ω angles are less than half of 2θ (an extreme case is GI-XRD), the footprint on the specimen surface becomes wide. The detector should receive the diffracted X-rays with a wide cross section due to the projection effect. For this situation, parallel slit analyzers or analyzer crystals are required as the receiving optics in combination with the detector in 0D mode. For the case where the ω angles are greater than half of 2θ , the cross section of the diffracted X-rays becomes narrow, and the 1D mode of the detector is useful for measuring RSM (the area of measurement is shown in blue) with high scan speeds.

In-plane RSMs (the area of measurement is shown in green) are measured with the detector in 0D mode in combination with in-plane parallel slit analyzers.

2.2. (La,Sr)MnO₃/ZnO double heterostructure on sapphire⁽⁴⁾

The result of XRD analysis of a (La, Sr)MnO₃/

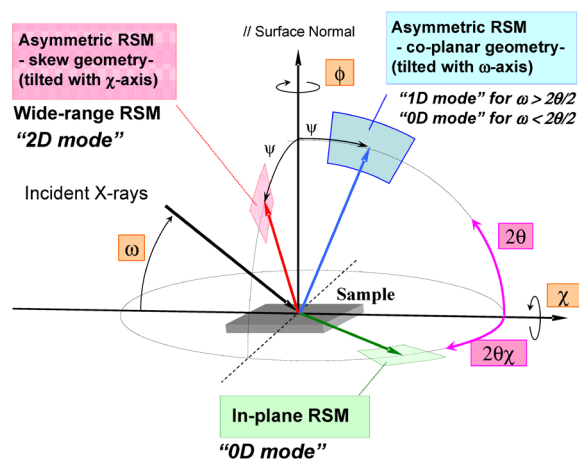


Fig. 1. Geometries of Reciprocal space mapping using a multidimensional detector.

* X-ray Research Laboratory, Rigaku Corporation.

2.3. Epitaxial growth of α -MoO₃ on sapphire^{(13), (14)}

The result of XRD analysis for the α -MoO₃ epitaxial film grown by the MBE (Molecular Beam Epitaxy) technique on Sap (0001) substrates is presented in this section.

MoO₃ is a wide-bandgap semiconductor oxide material that has been studied for various applications, such as Smart windows utilizing its electrochromic properties, ReRAM (Resistive Random Access Memory), or catalyst applications. MoO₃ exhibits polymorphism, where the orthorhombic α -MoO₃ phase is stable at high temperatures and the monoclinic β -MoO₃ phase is stable at low temperatures. We have succeeded in growing high quality epitaxial thin films of α -MoO₃ phase on Sap (0001) substrates and reported their crystalline quality and electrical/optical properties^{(13), (14)}. We recently also succeeded in growing high quality WO₃ epitaxial films on *r*-plane Sap substrates with a thin α -MoO₃ buffer layer⁽¹⁵⁾. Details of growth conditions can be found in articles (13)–(15).

From θ - 2θ scans taken with the detector in 0D mode, it was confirmed that (010) of α -MoO₃ films grows parallel to (0001) of Sap substrates. Note that the orthorhombic space group setting of *Pbnm* ($a=3.96290$ Å, $b=13.8649$ Å, $c=3.69756$ Å)⁽¹⁶⁾ is employed in this article. The *b*-axis for α -MoO₃ films in this setting is perpendicular to the double-sheet layer of the Mo–O atomic network arrangements in the α -MoO₃ structure (Fig. 5).

With in-plane RSM measurements, the epitaxial orientation relationship between α -MoO₃ and Sap were revealed as follows:

$[100](010)\alpha\text{-MoO}_3 // [1\bar{1}00](0001)$ Sap

or simultaneously,

$[001](010)\alpha\text{-MoO}_3 // [11\bar{2}0](0001)$ Sap.

Considering the differences in rotational symmetries at the interface plane between (010) of α -MoO₃ (2-fold) and (0001) of Sap (6-fold), three possible orientations for the α -MoO₃ lattices should be taken into account. This situation is schematically illustrated in Fig. 6.

A wide-range RSM was performed with the detector

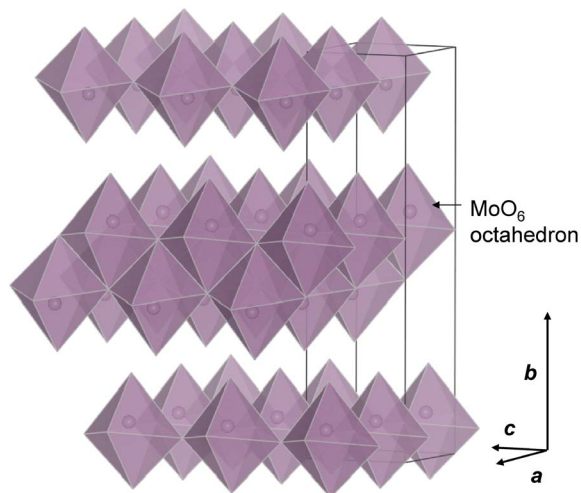


Fig. 5. Double-sheet layered structure model of α -MoO₃.

in 2D mode to reconfirm the epitaxial orientation relationship between α -MoO₃ and Sap. The data is shown in Fig. 7, where peaks from the α -MoO₃ epitaxial layer are marked with red circles. The vertical axis (q_z) in the figure is parallel to the [0001] axis of Sap, and the horizontal axis (q_x) is parallel to the [0 $\bar{1}$ 10] axis of Sap.

The unit cell axis lengths for α -MoO₃ were determined to be $a=3.957$ Å \pm 0.001 Å, $b=13.903$ Å \pm 0.001 Å, $c=3.609$ Å \pm 0.001 Å. The axes within the interface plane (*a*- and *c*-axis) showed slight contraction, while the *b*-axis perpendicular to the interface plane showed slight expansion, possibly caused by the lattice mismatch between the α -MoO₃ epitaxial film and the Sap substrate.

The diffraction/extinction rules for α -MoO₃ peaks were analyzed and the result is summarized in Table 1, together with rules expected from a crystal structure model with the space group setting of *Pbnm*. As can be seen from the table, the diffraction/extinction rules for α -MoO₃ observed peaks did not follow the rule expected from a crystal structure model with *Pbnm* setting. This fact indicates that the crystal structure of our α -MoO₃ epitaxial film is not compatible with one of *Pbnm* setting.

In order to explain this discrepancy, two possibilities are speculated so far. One is the stabilization of a metastable phase of MoO₃ with slight modification of atomic arrangements from a crystal structure model with *Pbnm* setting. Another possibility is that structural modification may happen due to the intercalations of light element species (H, OH etc.) into the double-sheet layers of the α -MoO₃ structure. Bursill et al.⁽¹⁷⁾ reported a modification of the α -MoO₃ structure by convergent beam electron diffraction analysis for ultra-thin single crystals of α -MoO₃. They revealed the breakdown of extinction rules due to the formations of stacking faults. They also suggested a model for the structural modification of α -MoO₃ structure caused by the intercalations of H ions. Further studies on this issue are underway.

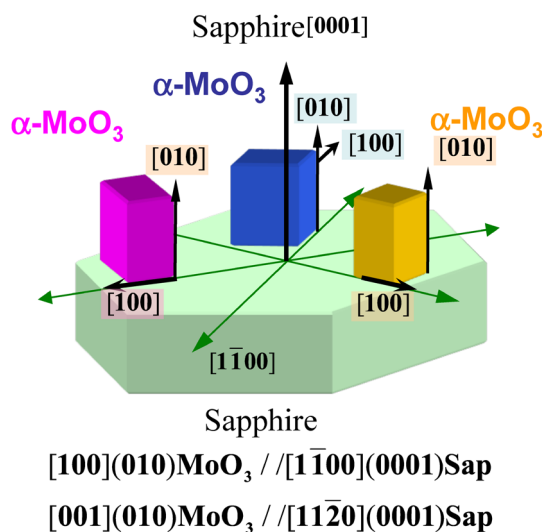


Fig. 6. Three possible variants of orientations for α -MoO₃ lattices on Sap(0001).

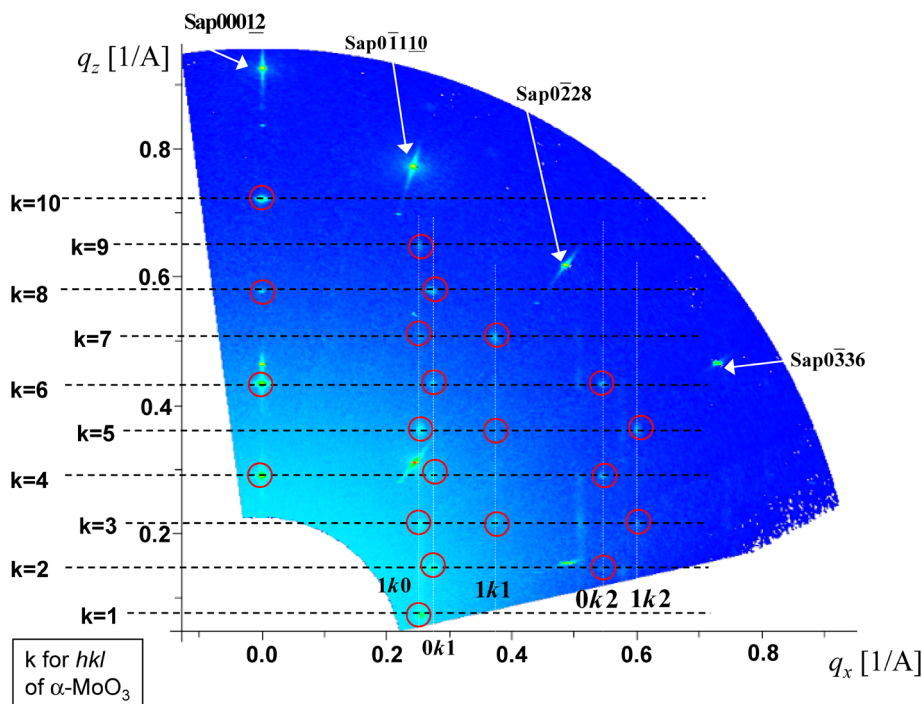


Fig. 7. Wide range RSM data for α -MoO₃/Sap. Peaks for α -MoO₃ epitaxial films are marked with red circles.

Table 1. Observed peaks in wide range RSM and expected diffraction conditions for peaks of α -MoO₃.

	Observed	Expected Diffraction condition (with Pbnm setting)
$0k0$	$k=2n$	$k=2n$
$1k0$	$k=2n+1$	No constraint
$0k1$	$k=2n$	$k=2n$
$1k1$	$k=2n+1$	No constraint
$0k2$	$k=2n$	$k=2n$
$1k2$	$k=2n+1$	No constraint

3. Conclusion

The results of XRD studies using multidimensional detectors, especially in 2D mode, were introduced in this article. The target materials were modern functional thin films, epitaxially grown on single crystal substrates. A wide-range RSM measurement with the detector in 2D mode is a powerful tool for the characterization of epitaxial thin films with complex domain structures. The analytical results will be more reliable and comprehensive when this approach is coupled with other approaches, such as RSM measurements with the detector in 1D mode, or with pole figure or in-plane measurements (including in-plane RSMs) with the detector in 0D mode.

Rigaku's Hypix-3000 installed on SmartLab systems is a multidimensional detector. The XRD measurements above can all be seamlessly performed without remounting detectors. It will greatly assist the XRD analysis on a variety of modern functional thin films.

References

- (1) K. Inaba: *Rigaku Journal (English Version)*, **30** (2014), No. 1, 1–6.
- (2) S. Kobayashi and K. Inaba: *Rigaku Journal (English Version)*, **32** (2016), No. 2, 1–5.
- (3) S. Kobayashi and K. Inaba: *Rigaku Journal (English Version)*, **26** (2010), No. 1, 1–11.
- (4) K. Inaba, S. Kobayashi, K. Uehara, A. Okada, S. L. Reddy and T. Endo: *Adv. Mater. Phys. Chem.*, **3** (2013), 72–89. (**Open Access**) <http://dx.doi.org/10.4236/amc.2013.31A010>
- (5) T. Endo, K. Uehara, T. Yoshii, M. Yokura, H. Zhu, J. Nogues, J. Colino and K. Endo: *Trans. Mater. Res. Soc. Jpn.*, **20th Anniversary Special Issue** (2012), 65–76.
- (6) K. Uehara, A. Okada, A. Okamoto, M. Yokura, S. L. Reddy, S. Kobayashi, K. Inaba, N. Iwata, R. Philip, H. Kezuka, M. Matsui and T. Endo: *Jpn. J. Appl. Phys.*, **51** (2012), 11PG07-1–11PG07-4.
- (7) M. Renninger: *Acta Cryst.*, **8** (1955), 606–610.
- (8) J. M. Sasaki, L. P. Cardoso, C. Campos, K. J. Roberts, G.F. Clark, E. Pantos and M.A. Sacilotti: *J. Appl. Phys.*, **29** (1996), 325–330.
- (9) P. Zaumseil: *J. Appl. Cryst.*, **48** (2015), 528–532.
- (10) K. Inaba: *Rigaku Journal (English Version)*, **30** (2014), No. 1, 7–16.
- (11) V. Bhosle and J. Narayan: *Appl. Phys. Lett.*, **90** (2007), 101903-1–101903-3.
- (12) K. Nagao and E. Kagami: *Rigaku Journal (English Version)*, **27** (2011), No. 2, 6–14.
- (13) K. Koike, R. Wada, S. Yagi, Y. Harada, S. Sasa and M. Yano: *Jpn. Jour. Appl. Phys.*, **53** (2014), 05FJ02-1–05FJ02-4.
- (14) K. Inaba, S. Kobayashi, S. Yagi, M. Matsuo, K. Koike, Y. Harada, S. Sasa and M. Yano: IWZnO-2014, C08.
- (15) M. Yano, K. Koike, M. matsuo, T. Murayama, Y. Harada and K. Inaba: *Appl. Surf. Sci.*, **381** (2016), 32–35.
- (16) H. Negishi, S. Negishi, Y. Kuroiwa, N. Sato and S. Aoyagi: *Phys. Rev., B: Condensed Matter*, **69** (2004), 0641111-1–0641111-8.
- (17) L. A. Bursill, W. C. T. Dowell, P. Goodman and N. Tate: *Acta Cryst.,-A*, **34** (1978), 296–308.